Published in final edited form as:
Nanoscale. 2010 September 5; 2(10): 1884–1891. doi:10.1039/c0nr00173b.

High-performance nanostructured MR contrast probes

Fengqin Hu[a], **Hrushikesh M. Joshi**[b], **Vinayak P. Dravid**[*,b], and **Thomas J. Meade**[*,a]

[a]Department of Chemistry, Biochemistry and Molecular Biology and Cell Biology, Neurobiology and Physiology, and Radiology, Northwestern University, Evanston, IL 60208, USA

[b]Department of Materials Science & Engineering, International Institute for Nanotechnology, Northwestern University, Evanston, IL 60208, USA

Abstract

Magnetic resonance imaging (MRI) has become a powerful technique in biological molecular imaging and clinical diagnosis. With the rapid progress in nanoscale science and technology, nanostructure-based MR contrast agents are undergoing rapid development. This is in part due to the tuneable magnetic and cellular uptake properties, large surface area for conjugation and favourable biodistribution. In this review, we describe our recent progress in the development of high-performance nanostructured MR contrast agents. Specifically, we report on Gd-enriched nanostructured probes that exhibit T_1 MR contrast and superparamagnetic Fe_3O_4 and $CoFe_2O_4$ nanostructures that display T_2 MR contrast enhancement. The effects of nanostructure size, shape, assembly and surface modification on relaxivity are described. The potential of these contrast agents for *in vitro* and *in vivo* MR imaging with respect to colloidal stability under physiological conditions, biocompatibility, and surface functionality are also evaluated.

Introduction

During the past two decades, magnetic resonance imaging (MRI) has become a ubiquitous tool for biological molecular imaging and clinical diagnosis.[1–4] One of many significant advantages of MR imaging is the ability to acquire (3-D) tomographic information of whole tissue samples and animals with high spatial resolution and soft tissue contrast. In addition, images are acquired without the use of ionizing radiation [X-ray and computed tomography (CT)] or radiotracers [positron emission tomography (PET) and single photon emission computed tomography (SPECT)]. MRI is based on the response of proton spin in the presence of an external magnetic field when triggered with a radio frequency pulse. Under the influence of an external magnetic field, protons align in one direction. Upon application of the RF pulse, aligned protons are perturbed and subsequently relax to the original state. There are two independent relaxation processes: longitudinal and transverse relaxation which are typically used to generate the MR images.

Due to the varying water concentration and local environment, intrinsic contrast between organs and tissues can be observed.[1,5] Signal resolution can be enhanced with the use of contrast agents. MR imaging agents are paramagnetic molecular complexes [typically Gd(III) chelates] due to the seven unpaired electrons and symmetrical *s* ground state.[5] Areas enriched with Gd(III) complexes exhibit an increase in signal intensity and appear bright in T_1-weighted images.[1,5] Superparamagnetic iron oxide nanoparticles are another class of MR contrast agents that produce a decrease in signal intensity and appear dark in T_2-weighted

[*]tmeade@northwestern.edu; Fax: +1 847 491 3832; Tel: + 1 847 491 2481. [*]v-dravid@northwestern.edu; Fax: +1 847 467 6573; Tel: +1 847 467 136.

images.[6,7] The efficiency of a contrast agent to reduce T_1 or T_2 of water protons is referred to as relaxivity, and defined by the eqn (1).[5,8]

$$1/T_{1,2}=1/T^0_{1,2}+r_{1,2}C \quad (1)$$

Where $1/T_{1,2}$ is the observed relaxation rate in the presence of contrast agents, $1/T^0_{1,2}$ is the relaxation rate of pure water, C is the concentration of the contrast agents, and r_1 and r_2 are the longitudinal and transverse relaxivities, respectively. According to this equation, MR contrast agents with high relaxivity are desired to have effective contrast enhancement under low agent concentrations and hence reduce toxicity.

Nanostructures have attracted considerable attention recently in science and technology.[9] Nanostructure-based MR contrast agents with improved characteristics and added functionalities have been developed as a result of the rapid progress in nanotechnology.[8,10–13] There are two broad classes of nanostructure-based MR contrast agents: 1) paramagnetic complexes doped in nanostructured framework structures, such as silica,[11] nanotubes,[14,15] gold,[16] titanium dioxide,[17] nanodiamonds,[18] perfluorocarbon,[19,20] and 2) inorganic magnetic nanoparticles, which themselves act as MR contrast agents.[12] Compared to conventional paramagnetic agents, nanostructure-based agents have a number of advantages: 1) the magnetic properties of inorganic magnetic nanostructures can be tailored by size, shape, composition, and assembly. 2) nanostructure-based MR contrast agents show tuneable cellular uptake. The majority of Gd(III) complex are limited to the blood pool and extracellular space.[21] However, after conjugating Gd(III) complexes to gold nanoparticles, a greater than 50-fold increase in cell uptake compared to Gd(III)-DOTA (1,4,7,10-tetraazacyclododecane-1,4,7,10-tet-raacetic acid) was observed.[16] 3) nanostructure-based MR contrast agents have a large surface area per unit volume that can be conjugated with targeting molecules and other probes, thus achieving targeting and multimodal agents. 4) the nanoscale dimension and shape of the nanostructure-based MR contrast agents allow varying and favourable biodistribution.

In this short review, we introduce our recent progress on the development of high-performance nanostructured MR contrast agents. Specifically, we will focus on Gd-enriched nanostructured T_1 agents, new magnetic Fe_3O_4 particles and $CoFe_2O_4$ T_2 agents. The effects of nanostructure size, shape, assembly and surface modification on relaxivity are discussed. The potential of these contrast agents for *in vitro* and *in vivo* MR imaging with respect to colloidal stability under physiological conditions, biocompatibility, and surface functionality are evaluated.

Gd-enriched nanostructured T_1 MR contrast agents

As mentioned above, current Gd(III) complex contrast agents are typically restricted to the extracellular environment. With the advance of MR imaging techniques in providing cellular-scale spatial resolution, considerable research efforts have focused on the development of cell-permeable contrast agents.[22–25] Loading Gd(III) complexes in nanostructures is another efficient strategy to increase their cellular uptake efficiency due to the unique attributes of nanostructures. In addition, the introducton of nanostructures endows other modalities besides MRI, and hence achieves prospects for multimodal probes.

TiO_2 nanoparticles labeled with Gd(III) complexes

TiO_2 nanoparticles represent one of the most studied nanoparticle systems due to their unique photocatalytic, chemical and structural properties. Paunesku *et al.*[26] reported that TiO_2 nanoparticles decorated with oligonucleotides function in a targeted and therapeutic

capacity. Targeting is accomplished *via* oligonucleotide hybridization to an intracellular organelle's DNA sequence, and therapeutic activity is elicited by light-induced scission of the nanoparticle-bound DNA *via* a redox reaction. In our laboratory, we functionalized a DNA-labeled TiO_2 nanoparticles with Gd(III) complex contrast agents to produce a biocompatible and therapeutically active delivery scaffold that is detectable by MRI.

Gd(III)-DO_3A (1,4,7-tris(carboxymethylaza)cyclododecane-10 -azaacetylamide) was modified on the surface of the DNA-labeled TiO_2 nanoparticles through ortho-substituted enediol ligands (Fig. 1a–b).[17] The nanoconjugates yielded a relaxivity of 3.5 ± 0.1 mM^{-1} s^{-1} per Gd(III) ion (1.5 T), similar to clinical small molecule contrast agents.[5] On the basis of the Ti:Gd ratio acquired from ICP-MS, each individual nanoparticle has an average relaxivity of 61.0 ± 1.7 mM^{-1} s^{-1}.

After transfection of PC12 cells with the nanoconjugates, X-ray fluorescence (XRF) spectroscopy showed that the nanoconjugates are present in the cytoplasm but not the nuclear regions, due to the conjugated DNA oligonucleotides. Analysis of Ti and Gd fluorescence signals and toxicity assays revealed that the nanoconjugates are biologically stable. The cellular imaging capability of the nanoconjugates was examined using PC3M cells (Fig. 1c). T_1-weighted MR images reveal that the cells incubated with the nanoconjugates display a greater contrast over control cells.

Gold nanoparticles labeled with Gd(III) complexes

A new class of nanostructured cellular imaging agent has been developed in our lab that uses gold nanoparticles as carriers.[16] DNA–Gd(III) conjugates were prepared by covalently attaching Gd(III) complexes to DNA through *click* chemistry. Then, the conjugates were immobilized on the citrate-stabilized Au nanoparticles to obtain DNA–Gd(III)@Au (Fig. 2a). The ionic relaxivities at 1.5 T of the nanoconjugates were measured to be 16.9 and 20.0 mM^{-1} s^{-1} for 13 nm and 30 nm DNA–Gd(III)@Au, respectively. This represents a fourfold and fivefold increase over the unconjugated Gd(III) complex (3.2 mM^{-1} s^{-1}),respectively. Taking into account the loading of Gd(III) per particle, the 13 nm DNA–Gd(III)@Au exhibited relaxivity of approximately 5779 mM^{-1} s^{-1} per particle, demonstrating that DNA–Gd(III)@Au is a highly efficient T_1 MR probe.

NIH/3T3 and Hela cell experiments showed that the Gd(III) uptake was more than 50-fold higher for DNA–Gd(III)@Au compared to Gd(III)–DOTA at all concentrations. On average, cells absorbed up to 10^6–10^7 Gd(III) ions per cell using only μM Gd(III) incubation concentrations. Compared with previous cell-permeable contrast agents using either the small transduction molecule stilbene and oligomeric polyarginine-conjugated Gd(III)–DOTA, DNA–Gd(III)@Au exhibits a very efficient means to label cells.[23,24] The high relaxivity and cellular uptake efficiency of DNA–Gd(III)@Au allow that μM Gd(III) incubation concentrations of DNA–Gd(III)@Au were sufficient to produce significant T_1-weighted contrast enhancement of small cell populations (Fig. 2b). These results represent the lowest reported incubation concentration of a Gd(III) complex or conjugate to produce a greater than 40% reduction of T_1 in cell pellets. Furthermore, the DNA–Gd(III)@Au is resistant to nuclease degradation which is important for long term cell tracking.[27]

This synthesis can be modified to introduce fluorescent dyes such as Cy3 on the nanoconjugates and to produce multimodal probes (Fig. 2a). The fluorescence micrographs show that the Cy3-DNA–Gd(III)@Au localize in small vesicles in the perinucleur region, suggesting that the nanoconjugates are taken up through an endocytic mechanism (Fig. 2c).

Nanodiamond particles labeled with Gd(III) complexes

Significant interest has focused on carbon-based nanomaterials such as fullerenes and nanotubes for biological applications (biosensors, drug delivery) due to their physical, chemical, and biological properties. However, the biocompatibility of these compounds remains in question.[28] Diamond-based nanoparticles have gained attention as an alternative carbon nanomaterial because of their excellent biocompatibility that is due in part to lower induction of cellular oxidative stress than is observed with other carbon nanomaterials.[29–32] Imaging of nanodiamond particles has largely centered on optical with fluorescence spectroscopy.[30,31] We selected covalent modification of the nanodiamond surface for attachment of Gd(III) complexes to produce nanodiamonds detectable by MR imaging.[18] An amine functionalized Gd(III) complex with a six carbon linker was synthesized and coupled to the carboxylic acid groups on the nanodiamond surface (Fig. 3a–b). ICP-MS analysis showed that 48 ± 3 μM of Gd(III) adhered to nanodiamonds per 1 mg/mL nanodiamond reaction.

The Gd(III)-modified nanodiamond particles significantly reduced the T_1 of water protons with a per Gd(III) relaxivity of 58.82 ± 1.18 $mM^{-1}s^{-1}$ at 1.5 T. This represents a tenfold increase compared to the monomer Gd(III) complex (r_1 5.42 ± 0.20 $mM^{-1}s^{-1}$) and is among the highest per-Gd(III) relaxivities ever reported. This enhanced contrast is clearly seen in the MR images of Gd(III)-modified and unmodified nanodiamond particles (Fig. 3c). The combination of interaction of the water nanophase, which is induced by the strong electrostatic potentials on the nanodiamond facets, with the paramagnetic metal and the size of the nanodiamond clusters (130 nm − 55 nm) may be the contributions for the high relaxivity of the system.

Superparamagnetic nanostructured T_2 MR contrast agents

Over the past two decades, dextran-coated superparamgnetic iron oxide (SPIO) and related nanoparticles (*e.g.*, CLIO, Feridex, Resovist, and Combidex) have been used as conventional T_2 MR contrast agents in clinical imaging and molecular imaging.[33,34] However, these magnetic nanoparticles exhibit low mono-dispersity and poor crystallinity due to the inherent disadvantages of co-precipitation synthesis method. To improve MR contrast effect, researchers have been developing new synthesis procedures for high-performance superparamagnetic nanostructured MR probes. The thermal decomposition method is one of the most developed and frequently utilized methods to produce monodispersed and highly crystalline magnetic nanostuctures.[10,35–38] The magnetic nanostructures synthesized through this procedure are typically coated with hydrophobic ligands and hence water insoluble. It is necessary to transfer the hydrophobic nanostructures from organic phase to aqueous phase.

To reach this goal, several strategies have been developed. These include ligand exchange, introduction of amphiphilic molecules and coating with a hydrophilic shell.[10] To avoid cumbersome phase transfer processes, novel one-pot processes have been developed to synthesize water-dispersible nanostructures with well-defined shape and controlled sizes.[13,39,40] For example, Gao group[13,39] synthesized a series of water-soluble and biocompatible Fe_3O_4 nanoparticles using polar solvent in a one-pot reaction. In this context, we developed several facile synthesis procedures for water-soluble, high-performance magnetic nanostructures. We have investigated the effect of size, shape, assembly and surface modification on MR relaxivities and the potential of these contrast agents for *in vitro* and *in vivo* MRI with respect to colloidal stability under physiological conditions, biocompatibility, and surface functionality.

Nanostructured Fe_3O_4

Enhancing *in vivo* targeting specificity is a great challenge encountered with iron oxide MR contrast agents. Commonly used iron oxide nanoparticle contrast agents generate local contrast through nonspecific uptake by mononuclear phagocytes, and with a hydrodynamic size of over 50 nm, these particles remain primarily intravascular and are taken up by the reticuloendothelial system (RES),[41,42] which severely undermines their targeting specificity. Smaller hydrodynamic sizes are desired to overcome these problems.[42,43] We have described a direct synthesis of monodisperse, water-soluble, 3–6 nm size Fe_3O_4 superparamagnetic nanoparticles *via* a one-pot reaction using iron(III) acetylacetonate [$Fe(acac)_3$] as the iron precursor and diethylene glycol (DEG) as the solvent, reducing agent, and stabilizer (Fig. 4a).[44] PEG modification of the surface of Fe_3O_4 nanoparticles is accomplished *via* a ligand-exchange reaction based on the relatively weak coordinating ability of DEG molecules.

Colloidal stability under physiological conditions is one of the most important issues in biological applications of nanomaterials. Fe_3O_4 nanoparticles synthesized through this procedure show excellent colloidal stability in phosphate buffered saline (PBS), fetal bovine serum (FBS), and calf bovine serum (CBS) (Fig. 4a). Furthermore, the Fe_3O_4 nanoparticles synthesized *via* this approach also tolerate high salt concentrations (≤ 1 M NaCl) and a wide pH range from 5 to 11.

As Fe_3O_4 nanoparticle nominal size increases from 3 to 4, 5, and to 6 nm, their r_2 gradually increases from 29 to 42, 48, and to 61 $mM^{-1}s^{-1}$, respectively. This size effect on relaxivity is due to surface spin-canting effects (*i.e.*, as the nanoparticle size decreases, the magnetically disordered spin-glass-like surface layer becomes more pronounced, and is reflected in the reduced net magnetic moment and MR contrast-enhancement effect).[10] In addition to size effects, surface modification plays an important role on relaxivity. Previous results showed that coordination chemistry of the inner capping ligand(s) and hydrophilicity of the coating layer are important factors to determine relaxivity.[45,46] Computer simulation results show that the coating layer that slows down water diffusion can also affect relaxivity (*i.e.*, as the thickness of this layer is increased, r_2 increases due to the increased volume of slowly diffusing water surrounding each nanoparticle).[47] Our experimental results clearly demonstrate this point. PEG modification of 3, 4, 5 and 6 nm Fe_3O_4 nanoparticles resulted in r_2 increases from 29 to 47, 42 to 69, 48 to 86, and 61 to 119 mM^{-1} s^{-1}, respectively, since PEG-Fe_3O_4 forms a larger water-slow diffusion layer than DEG-Fe_3O_4, as has been shown by DLS (Fig. 4b). This difference can be seen on the T_2-weighted MR images (Fig. 4c). *in vitro* experiments showed that DEG- and PEG-coated Fe_3O_4 nanoparticles have little effect on NIH/3T3 cell viability.

We have developed a simple one-step process for synthesis of amine-stabilized iron oxide nanoparticles from a single $FeCl_2$ precursor using dodecylamine (DDA) as the reducing and surface-functionalizing agent.[48] In this report, we have demonstrated that DDA electrostatically complexes with aqueous iron ion, reduces it and caps the nanoparticles. As such DDA does not dissolve in water at room temperature; however, reaction takes place immediately after it reaches 35 °C, forming highly dispersive Fe_3O_4 nanoparticles. In contrast, similar results were not observed at 100 °C. This observation suggests that reactivity of reaction strongly dependent on the nature of the amine group. It indicates that iron oxide nanoparticles were produced *via* Fe(II)-amine complex followed by its thermal decomposition. The reaction was so rapid that Fe_3O_4 were strongly protected by multlayers of amine molecules to avoid aggregation of nanoparticles. Capping of iron oxide nanoparticles with the amine molecules stabilizes the particles in solution nearly covalently and renders them water-dispersible. Higher dodecylamine concentrations and longer

reaction times lead to more stable, monodisperse nanoparticles with high relaxivity, for use in biomedical applications.

Spherical and faceted irregular (FI) $CoFe_2O_4$ nanostructures

Shape properties of MR contrast enhancement are not well understood. To investigate these effects, we synthesized spherical and FI $CoFe_2O_4$ *via* a high temperature solution phase method (Fig. 5a–b).[49] Since thermal activation and MRI properties of the cobalt ferrite nanostructures are well studied and easily quantifiable, we have used it to determine its shape dependent properties in spite of the fact that cobalt is toxic in nature. Spherical $CoFe_2O_4$ of various sizes were synthesized with the help of seed mediated growth in the organic phase, while FI $CoFe_2O_4$ was synthesized with the same method but in the presence of a magnetic field. The stable cobalt ferrite nanostructures of various shapes and sizes were phase transferred from the organic phase to the aqueous phase using 11-amino undecanoic acid.

Similar to Fe_3O_4 nanoparticles, the r_2 of $CoFe_2O_4$ nano-structures increases with size (*i.e.*, from 110, 169 to 301 mM^{-1} s^{-1} for 6, 10 and 15 nm spherical $CoFe_2O_4$ and from 155 to 345 mM^{-1} s^{-1} for 12 and 25 nm FI $CoFe_2O_4$). Furthermore, FI $CoFe_2O_4$ exhibits lower relaxivity than their spherical counterparts (Fig. 5c). However, with respect to their saturation magnetization, FI $CoFe_2O_4$ shows a higher relaxivity than spherical $CoFe_2O_4$, which might be due to the reduced magnetization induced by partial pinning of magnetic moments, pseudomagnetic charges because of corners and edges of the nanostructures and a greater surface-to-volume of FI $CoFe_2O_4$ (Fig. 5d). These results suggest that the relaxivity is not only dependent on the magnetic saturation of the $CoFe_2O_4$ but also affected by its morphology.

Superparamagnetic iron oxide nanoassemblies

Assembly of magnetic nanoparticles has two types of effects on the proton relaxation properties similar to random aggregates of magnetic nanoparticles.[8,50] One of them associates with the coarser structure of the nanoassemblies and magnetic field distribution around it, whereas the other one is limited to the inner part of the nanoassemblies (Fig. 6). The coarser effect dominantly influences r_2, while the inner one does not influence r_2 significantly but mainly affects r_1. The enhancement of r_1 produced by magnetic nanoparticles requires intimate contact between water molecules and the surface of the magnetic nano-particles similar to T_1 contrast agent based on Gd(III). Assembly of magnetic nanoparticles decreases the surface of magnetic nanoparticles in contact with the water and hence decreases the effect of inner sphere relaxation effect which in turn decreases the r_1 value.

In regard to T_2 contrast enhancement, due to the synergistic interactive magnetism arising from multiple magnetic nano-particles in the assembly, magnetic nanoparticle assemblies present higher r_2 than separated nanoparticles. The r_2 of the nanoassemblies can be expressed as:[50]

$$r_2 = \left(\frac{64\pi}{135}\right)\left(\mu N_g \frac{L(x)}{4\pi}\right)^2 \frac{N_A C_a}{R_a D} \quad (2)$$

where μ = magnetic moment of the nanoparticle, N_g = number of nanoparticles in an assembly, $L(x)$ = Langevin function, N_A = Avogadro's number, C_a = concentration of the assembly, R_a = radius of an assembly, and D = water diffusion coefficient. According to the above equation, r_2 is proportional μ and N_g. The overall effects of assembly on r_1 and r_2

increase the r_2/r_1 value and hence, produce high-efficiency T_2 contrast agents. Unlike increasing nanoparticle size to increase r_2, which will induce the superparamagnetic-ferromagnetic transition and no longer result in dispersibility of the nanoparticles in solution, the strategy of forming clusters of magnetic nanoparticles has the advantage of increasing r_2 while retaining the superparamagnetic properties.[51]

We have synthesized a series of water-soluble Fe_3O_4 magnetic nanoassemblies through heating a mixture of $Fe(acac)_3$, HOOC–PEG–COOH, and oleylamine in phenyl ether (Fig. 7a).[52] The presence of PEG on the Fe_3O_4 nanoassemblies was demonstrated by FTIR. PEG has been demonstrated to be a good choice to act as surfactant because it can stabilize nanoparticles in a wide pH range due to hydrogen bonding between PEG and water. Furthermore, PEG layers have been shown to be non-toxic, non-immunogenic, non-antigenic and protein-resistant.[53]

Consequently, PEG-coated Fe_3O_4 nanoassemblies synthesized through the above procedure show excellent colloidal stability in H_2O, PBS, cell culture media and serum, and tolerate a high salt concentration (1 M NaCl) and a wide pH range from 3 to 11 (Fig. 7a). The hydrodynamic sizes and T_2 values of the Fe_3O_4 nanoassemblies present an excellent stability during the three week measurement period. The presence of surface free carboxylic acid groups was demonstrated by zeta potential results, allowing further conjugation reactions with targeting molecules or other modalities.

At 250 K, the Fe_3O_4 nanoassemblies exhibit super-paramagnetic behavior without magnetic hysteresis and remanence. The saturation magnetizations of 42, 30 and 19 nm Fe_3O_4 nanoassemblies at 250 K are 33, 45, 36 emu g^{-1} Fe, respectively. This trend is consistent with that of the primary Fe_3O_4 nano-particle size in the Fe_3O_4 nanoassemblies (i.e., 4.3, 4.8 and 4.5 nm for 42, 30 and 19 nm Fe_3O_4 nanoassemblies, respectively). The r_2 values of 42, 30 and 19 nm Fe_3O_4 nanoassemblies at 1.5 T are 148, 238, and 126 mM^{-1} s^{-1}, respectively.

The contrast enhancement differences are due to the synergistic effects of the primary Fe_3O_4 nanoparticle size and the number of nanoparticles per Fe_3O_4 nanoassembly as shown in eqn (2) and can be seen on the T_2-weighted MR images (Fig. 7b). For comparison, the r_2 of 30 nm Fe_3O_4 nanoassemblies (238 mM^{-1} s^{-1}, 1.5 T) is 2.3 times of that of the commercial Feridex (104 mM^{-1} s^{-1}, 1.5 T) which has a similar primary particle size.[54] Furthermore, these Fe_3O_4 nanoassemblies with excellent colloidal stability and high transverse relaxivity have no effect on the viability of NIH/3T3 cells, indicating the Fe_3O_4 nanoassemblies are promising candidates as high-efficiency T_2 contrast agents for a variety of MR imaging applications.

Besides carboxylic acid functionalized Fe_3O_4 nanoassemblies, we developed a novel one-pot approach to prepare amine functionalized water-soluble Fe_3O_4 nanoassemblies. It is an environmentally and economically preferable one-step green chemistry approach using Fe-chloride precursors, biocompatible ethylene glycol as solvent and ethylenediamine as surfactants.[55,56] The size of the Fe_3O_4 nanoassemblies is about 40 ± 1 nm while that of the individual nanoparticles is about 6 nm. The Fe_3O_4 nanoassemblies exhibit superparamagnetic behavior and a high saturation magnetization of 64.3 emu g^{-1}. The r_2 of the Fe_3O_4 nanoassemblies is 314.6 mM^{-1} s^{-1}, which is 60% higher than that of 6 nm Fe_3O_4 nanoparticles and 2.7 times higher than that of commercial ferumoxytol. The presence of amine functional groups on the surface of the Fe_3O_4 nanoassemblies was confirmed by FTIR, thermal and elemental analyses, and provides an accessible surface for routine conjugation of biomolecules through well-developed bioconjugation chemistry.

Conclusions and outlook

Over last 20 years, nanostructure-based MR contrast agents have made remarkable progress. The two primary classes of nano-structure-based MR contrast agents include paramagnetic complexes doped in nanostructured frameworks and inorganic magnetic nanoparticles, which themselves act as MR contrast agents. The attachment of Gd(III) complexes to various nano-stuctures such as TiO_2, Au and nanodiamond particles not only retains or increases the MR contrast effect of the Gd(III) complex, but provides a scaffold to prepare multimodal probes and overcomes the extracelluar limitation of Gd(III) complexes and achieves cellular imaging agents. Further, the contrast enhancement effects of magnetic nanostructured T_2 contrast agents can be effectively tuned through size, shape, assembly or surface modification of the nanostructures.

Ultimately, one of the most significant obstacles of nano-structure agents is batch-to-batch reproducibility. Given the high performance of nanostructure-based MR contrast agents, a complementary understanding of their biological effects such as toxicity,[18] biodistribution[57] and pharmacokinetics[58] is required if the next stage (translational research) is to be successful.

Acknowledgments

We thank Dr Amanda L. Eckermann and Dr Mrinmoy De for helpful discussions. This work was supported by the Nano-materials for Cancer Diagnostics and Therapeutics under Grant 5 U54CA119341-02 and the National Institutes of Health/NIBIB Grant 1 R01EB005866-01.

Biographies

Dr Fengqin Hu received her Ph.D. degree in 2007 at the Institute of Chemistry, Chinese Academy of Sciences under the supervision of Prof. Mingyuan Gao. After that, she joined the group of Prof. Thomas J. Meade at Northwestern University as a postdoctoral fellow. Since 2010, she has been working in the Beijing Normal University as an Assistant Professor. Her research focuses on the synthesis of biocompatible inorganic nanocrystals as well as their biological and biomedical applications.

Dr Hrushikesh M. Joshi completed his Ph.D. under the supervision of Dr Murali Sastry, thereafter he worked with Prof. Satish Ogale for one year as a research associate at National Chemical Laboratory Pune. At present, he is working as CCNE postdoctoral research scholar at Northwestern University with Prof. Vinayak Dravid. His research interests include

synthesis and surface functionalization of inorganic nanoparticles for various industrial applications. He is recipient of the DST award for the meeting of Nobel laureate and students in chemistry, Lindau, Germany in 2006.

Vinayak P. Dravid is Professor of Materials Science & Engineering at Northwestern University, and founding Director of the NUANCE Center. His research program includes nanoscale dynamic phenomena in broad areas of nanostructured materials, energy, and convergence of engineering, physical and biomedical sciences. His awards include; Fellowships to Materials Research Society (MRS), Microscopy Society of America (MSA) and American Ceramic Society (ACerS). He is the recipient of the American Ceramic Society's Robert L. Coble Award and Richard M. Fulrath Award, MSA's Burton Medal, among other honors. He was elected twice to Northwestern Faculty Honor Roll for excellence in teaching.

Dr Thomas J. Meade is currently the Eileen Foell Chair in Cancer Research and Professor of Chemistry, Biochemistry and Molecular & Cell Biology, Neurobiology & Physiology, and Radiology, as well as the Director of the Center for Advanced Molecular Imaging (CAMI). Professor Meade's research focuses on bioinorganic coordination chemistry and biological molecular imaging, electron transfer processes and the development of electronic biosensors for the detection of DNA and proteins. He has founded three biotech companies developing hand-held devices for protein and DNA detection and bioactivated MR contrast agents for in vivo imaging of cancer.

References

1. Merbach, AE.; Toth, E. The Chemistry of Contrast Agents in Medical Magnetic Resonance Imaging. Wiley; New York: 2001.
2. Aime S, Cabella C, Colombatto S, Geninatti Crich S, Gianolio E, Maggioni F, Magn J. Reson. Imaging. 2002; 16:394–406.
3. Hu X, Norris DG. Annu. Rev. Biomed. Eng. 2004; 6:157–184. [PubMed: 15255766]
4. Winter Patrick M, Caruthers Shelton D, Wickline Samuel A, Lanza Gregory M. Curr. Cardiol. Rep. 2006; 8:65–69. [PubMed: 16507239]
5. Caravan P, Ellison JJ, McMurry TJ, Lauffer RB. Chem. Rev. (Washington, D.C.). 1999; 99:2293–2352.
6. Mendonca Dias MH, Lauterbur PC. Magn. Reson. Med. 1986; 3:328–330. [PubMed: 3713497]
7. Semelka RC, Helmberger TK. Radiology. 2001; 218:27–38. [PubMed: 11152776]
8. Laurent S, Forge D, Port M, Roch A, Robic C, Vander Elst L, Muller RN. Chem. Rev. (Washington, DC, U.S.). 2008; 108:2064–2110.
9. Hochbaum AI, Yang P. Chem. Rev. (Washington, DC, U.S.). 2010; 110:527–546.
10. Jun, Y.-w.; Lee, J-H.; Cheon, J. Angew. Chem., Int. Ed. 2008; 47:5122–5135.
11. Taylor KML, Kim JS, Rieter WJ, An H, Lin W, Lin W. J. Am. Chem. Soc. 2008; 130:2154–2155. [PubMed: 18217764]
12. Na HB, Song IC, Hyeon T. Adv. Mater. (Weinheim, Ger.). 2009; 21:2133–2148.
13. Hu F, Wei L, Zhou Z, Ran Y, Li Z, Gao M. Adv. Mater. (Weinheim, Ger.). 2006; 18:2553–2556.
14. Richard C, Doan B-T, Beloeil J-C, Bessodes M, Toth E, Scherman D. Nano Lett. 2008; 8:232–236. [PubMed: 18088153]
15. Sitharaman B, Kissell KR, Hartman KB, Tran LA, Baikalov A, Rusakova I, Sun Y, Khant HA, Ludtke SJ, Chiu W, Laus S, Toth E, Helm L, Merbach AE, Wilson LJ. Chem. Commun. 2005:3915–3917.
16. Song Y, Xu X, MacRenaris KW, Zhang X-Q, Mirkin CA, Meade TJ. Angew. Chem., Int. Ed. 2009; 48:9143–9147.
17. Endres PJ, Paunesku T, Vogt S, Meade TJ, Woloschak GE. J. Am. Chem. Soc. 2007; 129:15760–15761. [PubMed: 18047347]
18. Manus LM, Mastarone DJ, Waters EA, Zhang X-Q, Schultz-Sikma EA, MacRenaris KW, Ho D, Meade TJ. Nano Lett. 2010; 10:484–489. [PubMed: 20038088]
19. Flacke S, Fischer S, Scott MJ, Fuhrhop RJ, Allen JS, McLean M, Winter P, Sicard GA, Gaffney PJ, Wickline SA, Lanza GM. Circulation. 2001; 104:1280–1285. [PubMed: 11551880]
20. Winter PM, Morawski AM, Caruthers SD, Fuhrhop RW, Zhang H, Williams TA, Allen JS, Lacy EK, Robertson JD, Lanza GM, Wickline SA. Circulation. 2003; 108:2270–2274. [PubMed: 14557370]
21. Major JL, Meade TJ. Acc. Chem. Res. 2009; 42:893–903. [PubMed: 19537782]
22. Allen MJ, Meade TJ. JBIC, J. Biol. Inorg. Chem. 2003; 8:746–750.
23. Allen MJ, MacRenaris KW, Venkatasubramanian PN, Meade TJ. Chem. Biol. 2004; 11:301–307. [PubMed: 15123259]
24. Endres Paul J, Macrenaris Keith W, Vogt S, Allen Matthew J, Meade Thomas J. Mol. Imaging. 2006; 5:485–497. [PubMed: 17150161]
25. Lee J, Burdette JE, MacRenaris KW, Mustafi D, Woodruff TK, Meade TJ. Chem. Biol. (Cambridge, MA, U.S.). 2007; 14:824–834.
26. Paunesku T, Vogt S, Lai B, Maser J, Stojicevic N, Thurn KT, Osipo C, Liu H, Legnini D, Wang Z, Lee C, Woloschak GE. Nano Lett. 2007; 7:596–601. [PubMed: 17274661]
27. Modo, MM.; Bulte, JWW. Molecular and Cellular MR Imaging. CRC; Boca Raton: 2007.
28. Jia G, Wang H, Yan L, Wang X, Pei R, Yan T, Zhao Y, Guo X. Environ. Sci. Technol. 2005; 39:1378–1383. [PubMed: 15787380]
29. Narayan RJ, Wei W, Jin C, Andara M, Agarwal A, Gerhardt RA, Shih C-C, Shih C-M, Lin S-J, Su Y-Y, Ramamurti R, Singh RN. Diamond Relat. Mater. 2006; 15:1935–1940.

30. Yu S-J, Kang M-W, Chang H-C, Chen K-M, Yu Y-C. J. Am. Chem. Soc. 2005; 127:17604–17605. [PubMed: 16351080]
31. Fu C-C, Lee H-Y, Chen K, Lim T-S, Wu H-Y, Lin P-K, Wei P-K, Tsao P-H, Chang H-C, Fann W. Proc. Natl. Acad. Sci. U. S. A. 2007; 104:727–732. [PubMed: 17213326]
32. Schrand AM, Dai L, Schlager JJ, Hussain SM, Osawa E. Diamond Relat. Mater. 2007; 16:2118–2123.
33. Weissleder R, Lee AS, Fischman AJ, Reimer P, Shen T, Wilkinson R, Callahan RJ, Brady TJ. Radiology (Easton, Pa.). 1991; 181:245–249.
34. Weissleder R, Moore A, Mahmood U, Bhorade R, Benveniste H, Chiocca EA, Basilion JP. Nat. Med. (N.Y.). 2000; 6:351–354.
35. Rockenberger J, Scher EC, Alivisatos AP. J. Am. Chem. Soc. 1999; 121:11595–11596.
36. Park J, An K, Hwang Y, Park J-G, Noh H-J, Kim J-Y, Park J-H, Hwang N-M, Hyeon T. Nat. Mater. 2004; 3:891–895. [PubMed: 15568032]
37. Jana NR, Chen Y, Peng X. Chem. Mater. 2004; 16:3931–3935.
38. Sun S, Zeng H, Robinson DB, Raoux S, Rice PM, Wang SX, Li G. J. Am. Chem. Soc. 2004; 126:273–279. [PubMed: 14709092]
39. Li Z, Chen H, Bao H, Gao M. Chem. Mater. 2004; 16:1391–1393.
40. Wan J, Cai W, Meng X, Liu E. Chem. Commun. 2007:5004–5006.
41. Moghimi SM, Hunter AC, Murray JC. Pharmacol. Rev. 2001; 53:283–318. [PubMed: 11356986]
42. Neuberger T, Schoepf B, Hofmann H, Hofmann M, Von Rechenberg B. J. Magn. Magn. Mater. 2005; 293:483–496.
43. Xie J, Chen K, Lee H-Y, Xu C, Hsu AR, Peng S, Chen X, Sun S. J. Am. Chem. Soc. 2008; 130:7542–7543. [PubMed: 18500805]
44. Hu F, MacRenaris KW, Waters EA, Liang T, Schultz-Sikma EA, Eckermann AL, Meade TJ. J. Phys. Chem. C. 2009; 113:20855–20860.
45. Duan H, Kuang M, Wang X, Wang YA, Mao H, Nie S. J. Phys. Chem. C. 2008; 112:8127–8131.
46. Daou TJ, Greneche JM, Pourroy G, Buathong S, Derory A, Ulhaq-Bouillet C, Donnio B, Guillon D, Begin-Colin S. Chem. Mater. 2008; 20:5869–5875.
47. LaConte Leslie EW, Nitin N, Zurkiya O, Caruntu D, O'Connor Charles J, Hu X, Bao G. J. Magn. Reson. Imaging. 2007; 26:1634–1641. [PubMed: 17968941]
48. Aslam M, Schultz EA, Sun T, Meade T, Dravid VP. Cryst. Growth Des. 2007; 7:471–475.
49. Joshi HM, Lin YP, Aslam M, Prasad PV, Schultz-Sikma EA, Edelman R, Meade T, Dravid VP. J. Phys. Chem. C. 2009; 113:17761–17767.
50. Roch A, Gossuin Y, Muller RN, Gillis P. J. Magn. Magn. Mater. 2005; 293:532–539.
51. Ge J, Hu Y, Biasini M, Beyermann WP, Yin Y. Angew. Chem., Int. Ed. 2007; 46:4342–4345.
52. Hu F, MacRenaris KW, Waters EA, Schultz-Sikma EA, Eckermann AL, Meade TJ. Chem. Commun. 2010; 46:73–75.
53. Qin J, Laurent S, Jo YS, Roch A, Mikhaylova M, Bhujwalla ZM, Muller RN, Muhammed M. Adv. Mater. (Weinheim, Ger.). 2007; 19:1874–1878.
54. Seo WS, Lee JH, Sun X, Suzuki Y, Mann D, Liu Z, Terashima M, Yang PC, McConnell MV, Nishimura DG, Dai H. Nat. Mater. 2006; 5:971–976. [PubMed: 17115025]
55. Barick KC, Aslam M, Prasad PV, Dravid VP, Bahadur D. J. Magn. Magn. Mater. 2009; 321:1529–1532. [PubMed: 20160860]
56. Barick KC, Aslam M, Lin Y-P, Bahadur D, Prasad PV, Dravid VP. J. Mater. Chem. 2009; 19:7023–7029.
57. Sun CR, Du K, Fang C, Bhattarai N, Veiseh O, Kievit F, Stephen Z, Lee DH, Ellenbogen RG, Ratner B, Zhang MQ. ACS Nano. 2010; 4:2402–2410. [PubMed: 20232826]
58. Oostendorp M, Douma K, Hackeng TM, van Zandvoort MAMJ, Post MJ, Backes WH. Contrast Media Mol. Imaging. 2010; 5:9–17. [PubMed: 20101742]

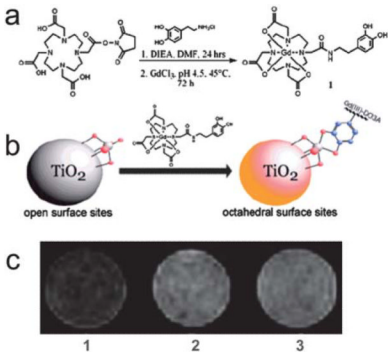

Fig. 1.

The scheme of (a) the synthetic route to a dopamine-modified MR contrast agent (DOPA-DO_3A) and (b) functionalization of DNA-labeled TiO_2 nanoparticles with DOPA-DO_3A; (c) T_1-weighted MR images of (1) control PC3M cells, (2) and (3) PC3M cells incubated with 0.001 mM DNA-DOPA-DO_3A-modified TiO_2 nanoconjugates with (2) 1.8% and (3) 4.4% 1:TiO_2 active site coverage (from ref. 17).

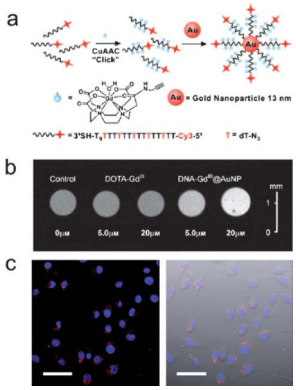

Fig. 2.

(a) Scheme of the synthesis of Cy3-DNA-Gd(III)@Au; (b) T_1-weighted MR images of NIH/3T3 cells incubated with DNA–Gd(III)@Au and Gd(III)–DOTA; (c) Confocal fluorescence micrographs of NIH/3T3 cells incubated with Cy3-DNA-Gd(III)@Au. Scale bar = 50 μm (from ref. 16).

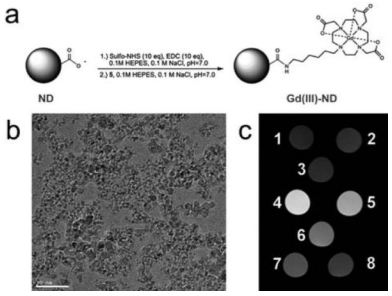

Fig. 3.

(a) Scheme of the conjugation of the Gd(III) contrast agent to the nanodiamond surface; (b) TEM image of the nanodiamond particles (scale bar = 50 nm); (c) T_1-weighted MR images of (1) water, (2) 1 mg/mL undecorated nanodiamond, (3) undecorated nanodiamond + coupling reagents, and (4)–(8) Gd(III)-modified nanodiamond particles with Gd(III) concentrations of 48, 38, 22, 10, and 5 μM, respectively (from ref. 18).

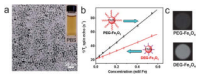

Fig. 4.

(a) TEM image of 6 nm DEG-Fe_3O_4; Inset is a photograph of the 6 nm DEG-Fe_3O_4 suspended in PBS; (b) T_2 relaxation rates ($1/T_2$) of 6nm PEG-Fe_3O_4 and 6 nm DEG-Fe_3O_4 at different Fe concentrations; (c) T_2-weighted MR images of 6 nm PEG-Fe_3O_4 and 6 nm DEG-Fe_3O_4 at Fe concentration of 7.5 mg/L (from ref. 44).

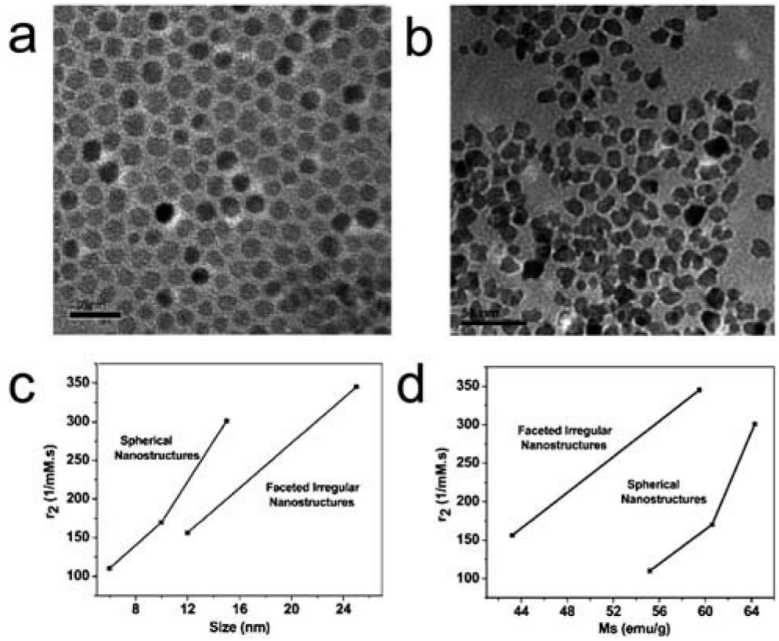

Fig. 5.

(a–b) TEM images of (a) 6 nm spherical and (b) 12 nm FI $CoFe_2O_4$ nanostructures; The scale bars in a and b are 20 nm and 50 nm, respectively; (c–d) Plot of relaxivities versus (c) size and (d) saturation magnetization of the $CoFe_2O_4$ nanostructures. (from ref. 49).

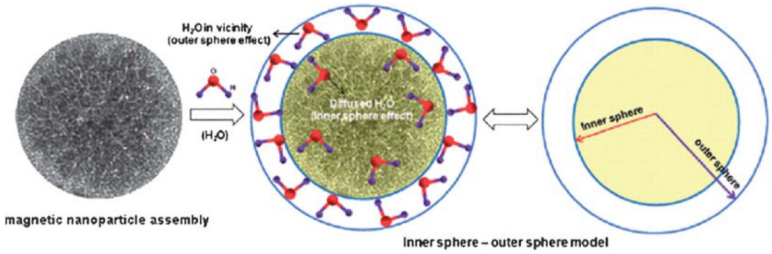

Fig. 6.
A schematic representation of outer sphere–inner sphere model of magnetic nanoparticle assembly (from ref. 56).

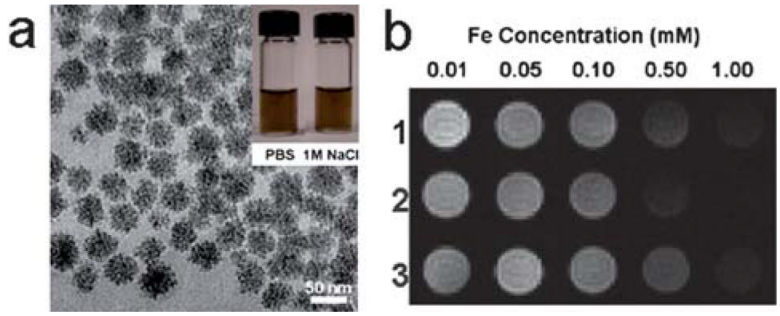

Fig. 7.

(a) TEM image of the 42 nm Fe_3O_4 nanoassemblies (scale bar = 50 nm); Inset are photographs of the Fe_3O_4 nanoassemblies suspended in PBS and 1 M NaCl.; (b) T_2-weighted MR images of aqueous solutions of (1) 42 nm, (2) 30 nm and (3) 19 nm Fe_3O_4 nanoassemblies at various Fe concentrations (from ref. 52).